

Electroencephalogram signatures of loss and recovery of consciousness from propofol

Patrick L. Purdon^{a,b,1}, Eric T. Pierce^a, Eran A. Mukamel^{c,d}, Michael J. Prerau^a, John L. Walsh^a, Kin Foon K. Wong^a, Andres F. Salazar-Gomez^a, Priscilla G. Harrell^a, Aaron L. Sampson^a, Aylin Cimenser^a, ShiNung Ching^{a,b}, Nancy J. Kopell^{e,1}, Casie Tavares-Stoekel^a, Kathleen Habeeb^f, Rebecca Merhar^a, and Emery N. Brown^{a,b,g,h,1}

^aDepartment of Anesthesia, Critical Care, and Pain Medicine, and ^fClinical Research Center, Massachusetts General Hospital, Boston, MA 02114; ^bDepartment of Brain and Cognitive Sciences, ^gDivision of Health Sciences and Technology, and ^hInstitute for Medical Engineering and Science, Massachusetts Institute of Technology, Cambridge, MA 02139; ^cCenter for Brain Science, Harvard University, Cambridge, MA 02139; ^dCenter for Theoretical Biological Physics, University of California at San Diego, La Jolla, CA 92093; and ^eDepartment of Mathematics and Statistics, Boston University, Boston, MA 02215

Contributed by Nancy J. Kopell, January 3, 2013 (sent for review September 22, 2012)

Unconsciousness is a fundamental component of general anesthesia (GA), but anesthesiologists have no reliable ways to be certain that a patient is unconscious. To develop EEG signatures that track loss and recovery of consciousness under GA, we recorded high-density EEGs in humans during gradual induction of and emergence from unconsciousness with propofol. The subjects executed an auditory task at 4-s intervals consisting of interleaved verbal and click stimuli to identify loss and recovery of consciousness. During induction, subjects lost responsiveness to the less salient clicks before losing responsiveness to the more salient verbal stimuli; during emergence they recovered responsiveness to the verbal stimuli before recovering responsiveness to the clicks. The median frequency and bandwidth of the frontal EEG power tracked the probability of response to the verbal stimuli during the transitions in consciousness. Loss of consciousness was marked simultaneously by an increase in low-frequency EEG power (<1 Hz), the loss of spatially coherent occipital alpha oscillations (8–12 Hz), and the appearance of spatially coherent frontal alpha oscillations. These dynamics reversed with recovery of consciousness. The low-frequency phase modulated alpha amplitude in two distinct patterns. During profound unconsciousness, alpha amplitudes were maximal at low-frequency peaks, whereas during the transition into and out of unconsciousness, alpha amplitudes were maximal at low-frequency nadirs. This latter phase–amplitude relationship predicted recovery of consciousness. Our results provide insights into the mechanisms of propofol-induced unconsciousness, establish EEG signatures of this brain state that track transitions in consciousness precisely, and suggest strategies for monitoring the brain activity of patients receiving GA.

General anesthesia (GA), a drug-induced state comprising unconsciousness, amnesia, analgesia, and immobility with maintenance of physiological stability (1, 2), is a cornerstone of modern medicine that is crucial for safely performing most surgical and many nonsurgical procedures. In the United States, nearly 60,000 people receive GA daily for surgery alone (1), suggesting that no physicians manipulate the state of the brain more often or more profoundly than anesthesiologists. Ironically, brain-state monitoring is not an accepted practice in anesthesia care because markers that reliably track changes in level of consciousness under GA have yet to be identified (3, 4). The standards for assessing if patients are adequately anesthetized include indirect measures of brain state—changes in heart rate, blood pressure, and muscle tone—along with presumed drug pharmacokinetics, pharmacodynamics, and, for inhaled anesthetics, the level of exhaled anesthetic gas.

The EEG, which measures scalp electrical potentials generated by cortical postsynaptic currents (5), has long been considered the most feasible approach for tracking brain states under GA. The first EEG recordings in humans under GA, reported in 1937, revealed systematic changes with increasing doses of both ether and pentobarbital (6). Despite attempts to characterize EEG morphology under GA (6–9), reading the EEG has not become part of routine anesthesiology practice. Instead, a simpler ap-

proach is used: Present-day depth-of-anesthesia monitors compute proprietary indices that reduce the EEG to a single, easy-to-interpret number intended to represent a patient's level of unconsciousness (10–15). These indices are designed to apply to all anesthetics and are constructed from a combination of spectral and entropy measures that typically require tens of seconds to compute (3, 16). Despite the appeal of this approach, these indices relate only indirectly to level of unconsciousness. Compared with non-EEG-based approaches, they have been ineffective in reducing the incidence of intraoperative awareness, i.e., when patients are aware under GA even though they appear to be unconscious (4). The need to develop principled neurophysiological approaches to monitoring the state of the brain under GA has become particularly compelling given growing concerns about its possible detrimental effects, including emergence delirium in children (17), adverse developmental effects in neonates and infants (18), and cognitive dysfunction in the elderly (19).

The black-box approach of these indices obscures structure in the EEG signal, visible even in 1937 (6), that could be related directly to the state of consciousness in the same way that the electrocardiogram, blood pressure, and cardiac output can be related to the state of the cardiovascular system. A variety of EEG patterns are known to arise during GA maintained by both GABA_A receptor-specific and ether-derived anesthetics. These EEG patterns include increases in frontal EEG power (20–24), a shift in EEG power toward lower frequencies (25), changes in coherence (22, 26), and burst suppression and isoelectricity (27). However, the relationship between these or other EEG patterns

Significance

Anesthesiologists reversibly manipulate the brain function of nearly 60,000 patients each day, but brain-state monitoring is not an accepted practice in anesthesia care because markers that reliably track changes in level of consciousness under general anesthesia have yet to be identified. We found specific behavioral and electrophysiological changes that mark the transition between consciousness and unconsciousness induced by propofol, one of the most commonly used anesthetic drugs. Our results provide insights into the mechanisms of propofol-induced unconsciousness and establish EEG signatures of this brain state that could be used to monitor the brain activity of patients receiving general anesthesia.

Author contributions: P.L.P., E.T.P., J.L.W., and E.N.B. designed research; P.L.P., E.T.P., J.L.W., A.F.S.-G., P.G.H., C.T.-S., K.H., R.M., and E.N.B. performed research; P.L.P., E.A.M., M.J.P., K.F.K.W., A.C., and E.N.B. contributed new analytic tools; P.L.P., E.A.M., M.J.P., K.F.K.W., A.F.S.-G., A.L.S., A.C., S.C., N.J.K., and E.N.B. analyzed data; and P.L.P. and E.N.B. wrote the paper.

Conflict of interest statement: P.L.P. and E.N.B. have a patent pending on anesthesia monitoring.

Freely available online through the PNAS open access option.

¹To whom correspondence may be addressed. E-mail: patrickp@nmr.mgh.harvard.edu, nk@bu.edu, or enb@neurostat.mit.edu.

This article contains supporting information online at www.pnas.org/lookup/suppl/doi:10.1073/pnas.1221180110/-DCSupplemental.

and the loss and recovery of consciousness remain poorly understood. In particular, it has been difficult to identify specific EEG signatures that are associated with the point of loss of consciousness (LOC), because most anesthesia-related EEG data come from clinical settings in which GA induction is performed rapidly, causing the crucial transition from consciousness to unconsciousness within 30–60 s (1). Compounding this rapid LOC is the problem of measuring level of consciousness. The most common approach is to ask patients to respond to a verbal or physical stimulus and rate the quality of responses on a 0–5 numerical scale (10, 28). This highly subjective assessment usually is repeated on a time-scale of minutes (10, 29) and resolves poorly the time point at which consciousness is lost or regained. EEG signatures that predict return of consciousness have been difficult to establish for similar reasons.

To study the relationship between EEG activity and the loss and recovery of consciousness, we recorded high-density (64-channel) EEGs while administering increasing (induction) and decreasing (emergence) doses of propofol to 10 healthy volunteers executing a structured auditory-response task to assess conscious behavior. Over an ~2-h period, we used a computer-controlled infusion to increase the target effect-site concentration of propofol gradually from a baseline of 0 $\mu\text{g}/\text{mL}$ to a peak level of 5 $\mu\text{g}/\text{mL}$ (30). We then gradually decreased the propofol target

effect-site concentration until it once again was 0 $\mu\text{g}/\text{mL}$ (Fig. 1A). During the infusion, subjects listened to prerecorded auditory stimuli, presented once every 4 s, consisting of their names, words, and a train of clicks. The subject's task was to identify the stimulus type with an appropriate button press. The time-series of responses provided a behavioral marker of the state of consciousness. We analyzed the EEG using time-varying spectral, coherence, and phase-amplitude methods and related these quantities to the probability of response to the auditory stimuli. We identified highly structured EEG signatures that can be used to monitor and manage the states of unconsciousness and sedation induced by propofol. These findings also provide insights into the mechanisms of propofol-induced unconsciousness.

Results

Continuous Transitions Between Consciousness and Unconsciousness.

To track changes in level of consciousness quantitatively in relation to propofol's target effect-site concentration (Fig. 1A), we used a Bayesian state-space algorithm (31) to estimate from the time-series of correct and incorrect responses each subject's response-probability curve for the verbal stimuli (neutral words and subject's name), P_{verbal} , and response-probability curve for the click stimuli, P_{clicks} (Fig. 1B). We used the same method to calculate the difference between the response-probability curves,

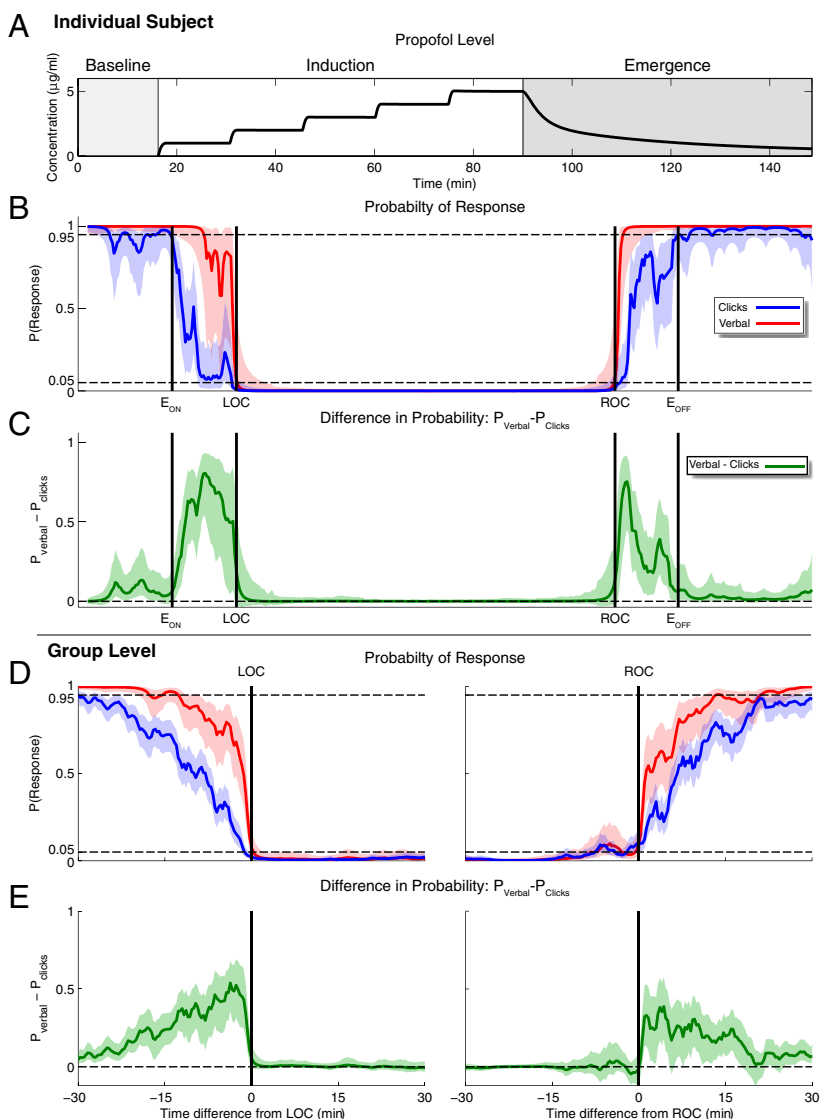


Fig. 1. Dynamics of the behavioral responses to the verbal and click stimuli during induction and emergence from propofol-induced unconsciousness. (A) The time course of the target effect-site concentrations of propofol during induction and emergence for subject 7. (B) Time courses of the response-probability curves for the click (blue, P_{clicks}) and verbal (red, P_{verbal}) stimuli and their respective 95% credibility intervals (shaded areas) for subject 7. The vertical black lines, from left to right, show E_{ON} , LOC, ROC, and E_{OFF} . (C) The curve of the difference between the verbal and click response-probability curves ($P_{\text{verbal}} - P_{\text{clicks}}$) and its associated 95% credibility interval for subject 7. (D) Group-level click (blue, P_{clicks}) and verbal (red, P_{verbal}) response-probability curves computed by aligning the individual subjects' response data during induction with respect to LOC and during emergence with respect to ROC. (E) Group-level curve for the difference between the verbal and click response-probability curves ($P_{\text{verbal}} - P_{\text{clicks}}$) and its 95% credibility intervals computed from the group-level curves in D. These results show that during gradual induction and emergence with propofol, loss and recovery of consciousness occur not instantaneously but gradually, and the probability of response depends critically on stimulus saliency.

$P_{verbal} - P_{clicks}$ (Fig. 1C). During induction P_{clicks} tended to decrease before P_{verbal} , whereas during emergence P_{verbal} tended to increase before P_{clicks} . To analyze this observation formally, we defined behavioral time markers for each subject, based on the P_{clicks} and P_{verbal} curves, to compare and pool data across subjects. We defined the first indication of a change in consciousness, the effect onset (E_{ON}), as the first time during induction at which P_{clicks} was less than 0.95 and remained so for at least 5 min. We chose a 5-min interval because it is approximately three times the equilibration time-constant for propofol (30). Similarly, we defined the effect offset (E_{OFF}) as the first time during emergence at which P_{clicks} was greater than 0.95 and remained greater for at least 5 min. We defined LOC as the first time during induction at which P_{verbal} was less than 0.05 and remained so for at least 5 min and return of consciousness (ROC) as the first time during emergence at which P_{verbal} was greater than 0.95 and remained so for at least 5 min.

We used Bayesian statistical inference to determine if $P_{clicks} < P_{verbal}$ by computing the posterior probability $\Pr\{P_{clicks} < P_{verbal}\}$. During induction, in 10 of 10 subjects, we observed that $P_{clicks} < P_{verbal}$ during the transition between E_{ON} and LOC; an example is shown in Fig. 1C. This condition is indicated by the fact that $\Pr\{P_{clicks} < P_{verbal}\} = \Pr\{0 < P_{verbal} - P_{clicks}\} > 0.95$, or equivalently, that the 95% credibility intervals for $P_{verbal} - P_{clicks}$ (shaded area in Fig. 1C) do not include 0 during this period. The transition between E_{ON} and LOC required a median of 23.9 min (minimum, 6.7 min; 25th percentile, 16.4 min; 75th percentile, 28.6 min; maximum 32.8 min). We estimated group-level P_{clicks} , P_{verbal} and $P_{verbal} - P_{clicks}$ curves for both induction and emergence by aligning the responses to the auditory tasks with respect to LOC and ROC, respectively (Fig. 1D and E). The group-level analysis corroborated the individual subject analyses, showing that $P_{clicks} < P_{verbal}$ during the transition to LOC ($\Pr\{P_{clicks} < P_{verbal}\} > 0.95$; Fig. 1E). Moreover, the group-level curves showed a gradual increase in the difference between these response probabilities as subjects approached LOC (Fig. 1E).

During emergence, individual response-probability curves were more variable, but again we found that $P_{clicks} < P_{verbal}$ at the group level ($\Pr\{P_{clicks} < P_{verbal}\} > 0.95$; Fig. 1E). During emergence, 6 of 10 subjects did not reach E_{OFF} because they did not achieve $P_{clicks} > 0.95$ for 5 min or longer. Therefore we conservatively estimated the emergence transition time by using either E_{OFF} or the end of the recording if E_{OFF} was not achieved. All subjects were conscious at the end of the recording time. We found that the transition between ROC and E_{OFF} required a median of 25.5 min (minimum, 4.9 min; 25th percentile, 12.8 min; 75th percentile, 38.0 min; maximum, 47.6 min). These results show that during gradual induction of and emergence from GA with propofol, loss and recovery of consciousness do not occur instantaneously but instead show gradual transitions during which the probability of response depends critically on stimulus saliency.

Dynamics of the EEG Spectrum Covary with Changes in Probability of Response and LOC/ROC. To analyze the dynamics of EEG oscillations during induction of and emergence from GA, we computed time-varying spectra (spectrograms) (32). We computed group-level spectrograms by taking the median baseline-normalized spectrogram across subjects, aligned at LOC for induction and at ROC for emergence (Fig. 2B). To minimize spatial blurring in this and subsequent analyses, we used a nearest-neighbor Laplacian reference, in which the Laplacian is calculated by taking each channel and subtracting the average of the nearest neighbors (24). During induction, gamma (25–40 Hz) and beta (13–24 Hz) power increased significantly above baseline levels during the 30 min before LOC—when $P_{clicks} < P_{verbal}$ —and remained elevated during the unconscious period (Fig. 2B and C). At LOC, both alpha (8–12 Hz) and low-frequency (0.1–1 Hz) power increased significantly (Fig. 2B and C). Fifteen minutes after LOC, the increases in alpha power were concentrated in frontal channels, whereas those for low-frequency power were

distributed broadly across temporal and parietal channels (Fig. 2D). During emergence, these changes in power occurred in reverse, following a similar time course: Frontal alpha and low-frequency power decreased at ROC, whereas gamma/beta power remained elevated throughout the post-ROC period when $P_{clicks} < P_{verbal}$. These analyses show that changes in broad-band gamma/beta power coincide with the behavior changes before LOC and after ROC, whereas changes in slow and alpha power coincide with LOC and ROC.

The standard definitions of the alpha, beta, and gamma EEG frequency bands provide a convenient shorthand for describing different oscillations. However, Fig. 2B makes clear that these propofol-induced oscillations are not confined neatly to single bands but instead move among these bands to varying degrees during both induction and emergence. Furthermore, when we examined individual subject spectrograms (e.g., Fig. S1), the broad-band gamma/beta power seen before LOC appeared to decrease continuously in frequency and bandwidth toward the alpha range, and then appeared to increase in frequency and bandwidth after ROC. To characterize this changing frequency distribution quantitatively, we estimated the median frequency and bandwidth (interquartile range) of the group-level baseline-normalized spectrograms in the frequency range between 2 and 40 Hz (Fig. 3A; see *SI Text* for additional details). We chose the 2–40 Hz interval to provide a broad range of frequencies while avoiding bias introduced by power in the low-frequency (0.1–1 Hz) band.

During induction, in the transition period before LOC, the median frequency decreased from 23.1 to 12.0 Hz, and the bandwidth decreased from 17.4 to 9.1 Hz (Fig. 3A). During emergence, in the transition period after ROC, the median frequency increased from 11.8 to 21.9 Hz, and the bandwidth increased from 9.9 to 12.8 Hz. We analyzed the spatial distribution of power at the median frequency at different behavioral time points for each subject and computed group-level spatial estimates at each time point by taking the median power across subjects. We used the previously defined behavioral time points (E_{ON} , LOC, ROC, and E_{OFF}), along with three newly defined time points—Pre-LOC (the midpoint between E_{ON} and LOC), Unconscious (the midpoint between LOC and ROC), and Post-LOC (the midpoint between ROC and E_{OFF})—to provide a higher temporal resolution in our analysis.

We found that the power at the median frequency had a frontal distribution across the different behavioral time points (Fig. 3B). To compare this spatial distribution of power at the median frequency with activity in the traditional frequency bands, we examined the spatial distribution of power within the gamma, beta, and alpha bands at the same time points (Fig. S2). Gamma and beta power showed a frontal distribution from Pre-LOC through LOC; during unconsciousness the frontal power distribution moved to the beta and alpha bands, consistent with the decreasing trend in the median frequency. During emergence, frontal power shifted from the alpha and beta bands to span the beta and gamma bands, again consistent with the increasing median frequency. In addition, frontal gamma power appeared to persist through E_{OFF} . These results show that activity in the gamma, beta, and alpha bands varies continuously during the transitions into and out of propofol-induced unconsciousness, and that power in these bands all have a common frontal distribution. To distinguish this pattern of continuously varying median frequency and bandwidth from activity within traditional fixed-frequency bands, we refer to this phenomenon as the “traveling peak.”

Changes in Spatially Coherent Alpha Activity Mark Unconsciousness. Because low-frequency and alpha oscillation power are prominent across the entire scalp and the frontal areas, respectively, during unconsciousness (Fig. 2D), we investigated the degree to which activity in these frequency bands was spatially coherent. We performed eigenvector decompositions of the cross-spectral matrices and analyzed the spatial distribution of the first eigenvector, or principal mode, at all frequencies from 0.1 to 40 Hz in

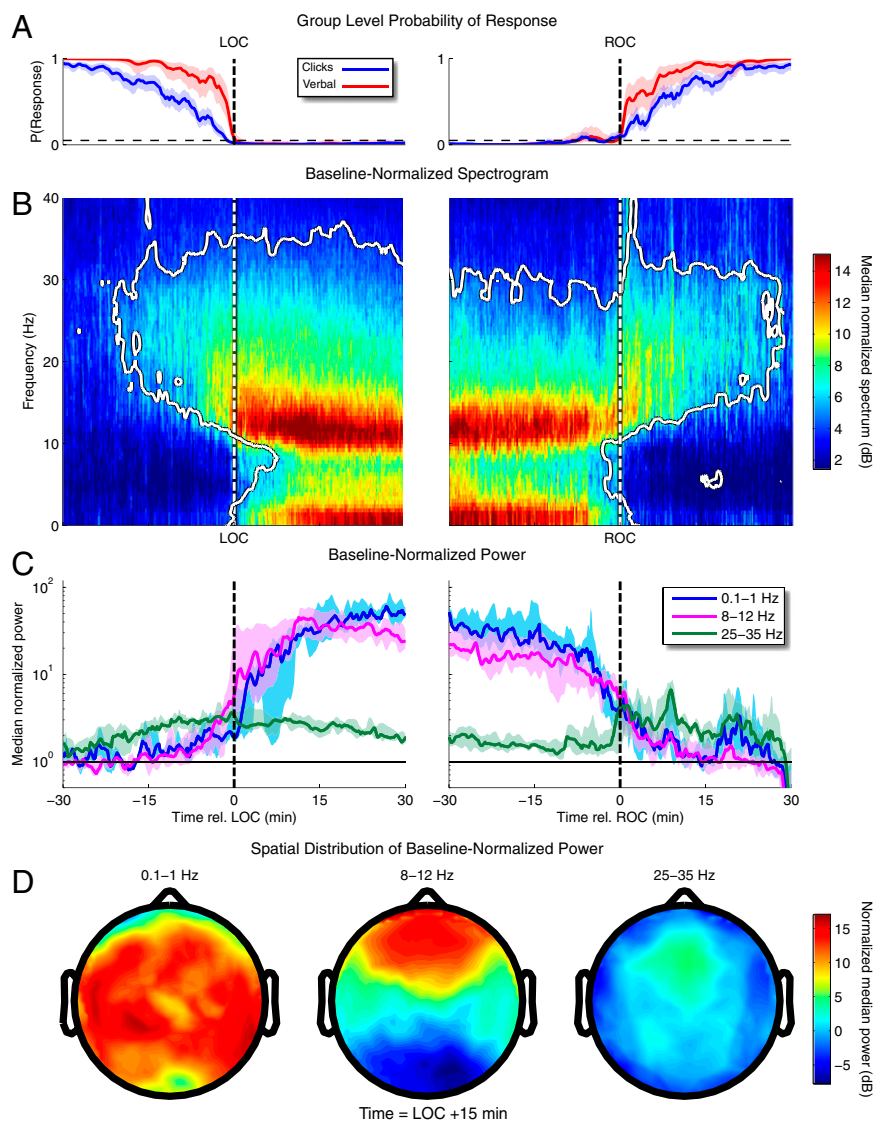


Fig. 2. Dynamics of the EEG spectrogram during induction and emergence from propofol-induced unconsciousness. (A) Group-level click (blue, P_{clicks}) and verbal (red, P_{verbal}) response-probability curves, as shown previously in Fig. 1D. (B) Group-level baseline-normalized spectrograms from a frontal channel (approximately Fz, nearest-neighbor Laplacian reference) aligned with respect to LOC and ROC. The white contour circumscribes the regions where power differs significantly from baseline ($P < 0.05$, sign test) and indicates significant increases in power spanning low-frequency (0.1–1 Hz) through gamma (25–35 Hz) bands. (C) Group-level time course of power in low-frequency, alpha (8–12 Hz), and gamma bands aligned with respect to LOC and ROC. (D) Group-level spatial distribution of low-frequency, alpha, and gamma power during unconsciousness (LOC + 15 min). These analyses show that changes in broad-band gamma/beta power coincide with the behavioral changes before LOC and after ROC, whereas changes in slow and alpha power coincide with LOC and ROC.

the baseline and unconscious states. We used the modal projection, i.e., the fraction of power explained by the principal mode at each frequency as a function of time, to measure the degree of coherent spatial activity (Fig. 4) (24, 32, 33). If a high fraction of the variance is explained by a principal mode, it suggests that there is highly coherent spatial activity at the associated frequency. We aligned the modal projection across subjects with respect to their respective LOCs and ROCs to construct group-level summaries (Fig. 4).

Only the principal mode in the alpha frequency band was prominent throughout the study (Fig. 4). At baseline, the alpha frequency had an occipital distribution because all subjects were instructed to keep their eyes closed throughout the study to avoid eye-movement artifacts and confounds (Fig. 4A and B). Hence, the occipital alpha is consistent with the well-known awake eyes-closed state (34). Occipital prominence of the principal mode was present while the subjects were awake, ended at LOC, and returned, and remained prominent after ROC. In contrast, during unconsciousness, the principal mode in the alpha range was prominent in a frontal distribution (Fig. 4C and D). Frontal prominence of the alpha principal mode occurred at the same time and frequency range (~ 10 Hz) as the increased frontal alpha power (Fig. 2) and the traveling peak (Fig. 3). In contrast, low frequencies did not show a prominent principal mode, even though low-frequency power increased by more than 10-fold in the

unconscious state compared with baseline (Fig. 2). These findings demonstrate that with propofol the transition from awake eyes-closed consciousness to unconsciousness is marked by the loss of spatially coherent occipital alpha oscillations and the appearance of spatially coherent frontal alpha oscillations. At ROC, the spatially coherent frontal alpha oscillations disappear and the spatially coherent occipital alpha oscillations return.

Different Patterns of Phase–Amplitude Modulation Mark Profound Unconsciousness and Recovery of Consciousness.

To investigate further the structure in the prominent low-frequency and alpha oscillations observed during unconsciousness, we analyzed phase–amplitude modulation between the rhythms (35). That is, we computed the extent to which the phase of the low-frequency oscillations modulated the amplitude of the alpha and beta (8–14 Hz) oscillations by computing time-varying phase–amplitude histograms for each subject and for the group aligned at LOC and ROC (36). As described in ref. 36 and in the *Materials and Methods*, we bandpass filtered the EEG signal to obtain low-frequency and alpha/beta components and used the Hilbert transform to estimate low-frequency phase and alpha and beta amplitude.

Our analysis identified two distinct patterns of phase–amplitude modulation. During induction, beginning ~ 20 min before LOC and extending ~ 10 min after LOC, the alpha/beta amplitudes were

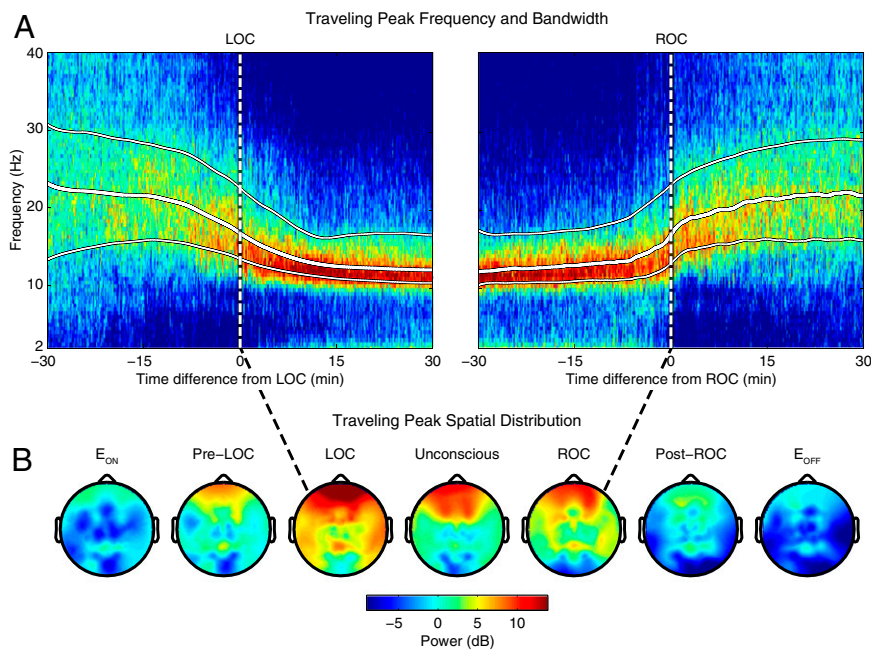


Fig. 3. Time course of the traveling peak, the continuous transformation in median frequency and bandwidth spanning the gamma, beta, and alpha bands during the transitions into and out of unconsciousness. (**A**) Group-level spectrograms computed between 2 and 40 Hz for a single frontal channel (approximately Fz, nearest-neighbor Laplacian reference), aligned with respect to LOC (*Left*) and ROC (*Right*) and normalized by the baseline spectrum. The 25th, median, and 75th percentiles within this frequency range are overlaid in white. The median represents the center frequency of the traveling peak, while the interquartile range (i.e., the difference between the 75th and 25th percentiles) represents the bandwidth of the traveling peak. (**B**) Spatial distribution of power at the median frequency at different behavioral endpoints. Pre-LOC is the midpoint between E_{ON} and LOC. Unconscious refers to the midpoint between LOC and ROC. Post-LOC is the midpoint between ROC and E_{OFF} .

largest at the troughs of low-frequency oscillations (Fig. 5B and C; $P < 0.05$ in 9 of 10 subjects within 10 min of LOC by permutation test, detailed in ref. 36; the troughs are Laplacian surface-negative deflections). We term this pattern “trough-max.” During profound unconsciousness, i.e., from 10–40 min after LOC, the phase–amplitude modulation shifted by 180° , such that the alpha/beta amplitudes were largest at the peaks of low-frequency oscillations (Fig. 5B and D; $P < 0.05$ in 8 of 10 subjects by permutation test; the peaks are Laplacian surface-positive deflections). We term this pattern “peak-max.” Both phase–amplitude modulation patterns were readily apparent in the raw EEG traces (Fig. 5C and D). During emergence, the phase–amplitude modulation reverted to the trough-max pattern at ~ 15 min before ROC (Fig. 5B; $P < 0.05$ in 9 of 10 subjects, permutation test). More generally, we found that the low-frequency oscillations modulated a range of frequencies from the theta band through the gamma band (Fig. S3).

Our findings suggest that the peak-max pattern is a marker of profound unconsciousness, and the transition from the peak-max pattern to the trough-max pattern predicts when subjects may be able to recover consciousness.

Discussion

The mechanisms of unconsciousness caused by GA are regarded as one of the great mysteries of medicine (37). By combining gradual induction and emergence with a task paradigm capable of tracking changes in behavior every 4 s, our study offers behavioral markers and EEG signatures characterizing loss and recovery of consciousness from propofol and mechanistic insights into how propofol may induce unconsciousness. Our findings are (i) the behavioral changes in the transitions between consciousness and unconsciousness depend critically on stimulus saliency; (ii) the median frequency and bandwidth of frontal EEG power (the

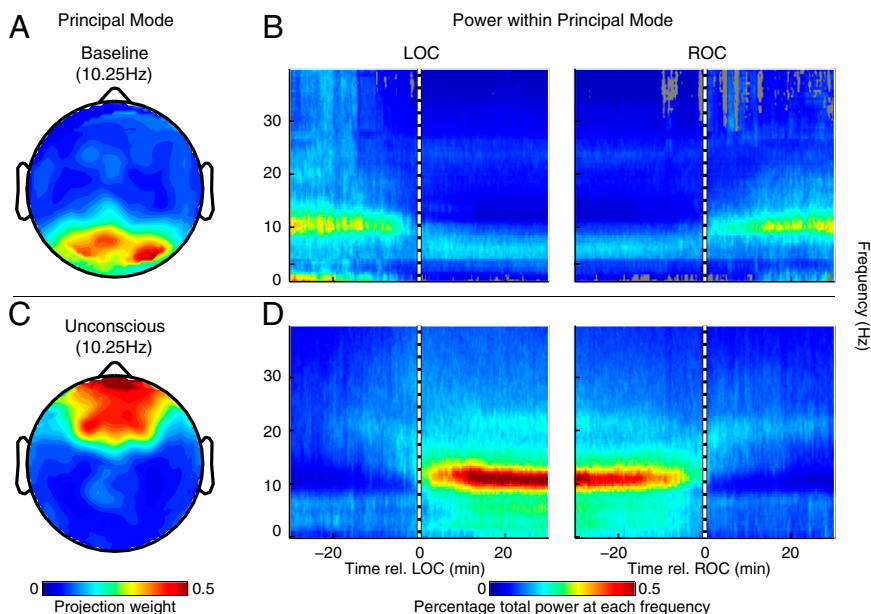


Fig. 4. Spatially coherent alpha oscillations at LOC and ROC. (**A**) At baseline, spatially coherent alpha oscillations are concentrated in occipital channels, represented by the principal mode of the cross spectral matrix. (**B**) Activity within the principal mode, represented by the modal projection (the proportion of total power captured by the principal mode) dissipates at LOC (*Left*) and returns at ROC (*Right*). (**C**) In the unconscious state, spatially coherent alpha oscillations are concentrated in frontal channels. (**D**) Activity within this frontal alpha mode, characterized by the modal projection, begins after LOC and ceases at ROC. Statistical significance for the modal projection was assessed using a permutation procedure (*Materials and Methods*); areas shaded in gray were not significant ($P > 0.05$). These analyses reveal that there is a change in coherent alpha oscillations at LOC, when a spatially coherent occipital alpha mode shuts off and a spatially coherent frontal alpha mode engages. These changes reverse at ROC.

A Phase-Amplitude Modulation

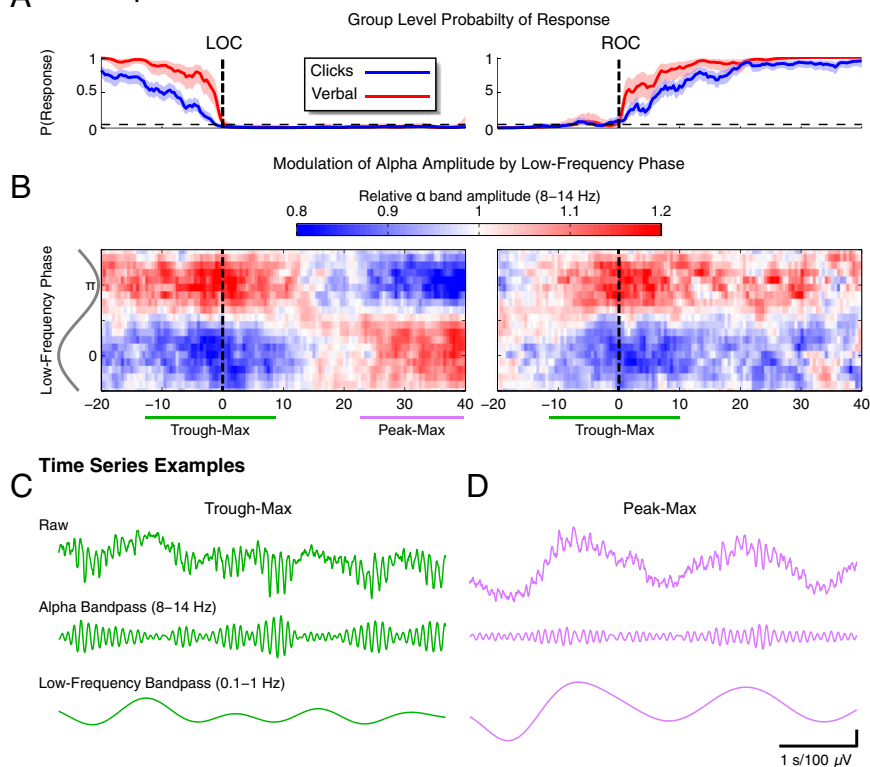


Fig. 5. Two distinct patterns of phase–amplitude modulation that develop asynchronously with LOC and ROC. (A) Group-level click (blue, P_{clicks}) and verbal (red, P_{verbal}) response-probability curves as shown in Fig. 1D. (B) The phase–amplitude histogram showing the relationship between the low-frequency (0.1–1 Hz) phase (y-axis, shown with reference sinusoid) and mean-normalized alpha/beta (8–14 Hz) oscillation amplitude (color map) as a function of time (x-axis) relative to LOC (Left) and ROC (Right). The trough-max pattern, in which the alpha oscillation amplitude is maximal at the low-frequency troughs, occurs during transitions into and out of unconsciousness. The peak-max pattern, in which the alpha oscillation amplitude is maximal at the low-frequency peaks, occurs during periods of profound unconsciousness. (C) The trough-max pattern observed in the time-domain EEG trace of an individual subject. (D) The peak-max pattern observed in the time-domain EEG trace of an individual subject. Modulograms and time-domain traces are from a frontal channel (approximately Fz, nearest-neighbor Laplacian reference). The peak-max modulation identifies a profound state of unconsciousness, whereas the trough-max pattern appears during transitions into and out of unconsciousness and therefore can be used to predict ROC.

traveling peak) track changes in level of consciousness; (iii) LOC is marked by an increase in low-frequency power, loss of coherent occipital alpha oscillations, and the appearance of coherent frontal alpha oscillations; (iv) ROC is marked by a decrease in low-frequency power, loss of coherent frontal alpha oscillations, and reappearance of coherent occipital alpha oscillations; (v) the trough-max pattern of phase–amplitude modulation marks the transitions into and out of unconsciousness, whereas the peak-max pattern marks profound unconsciousness. These behavioral and EEG signatures are summarized in Fig. 6.

Neurophysiological Properties of Propofol’s EEG Signatures. The findings from our traveling peak and principal mode analyses (Fig. 3A and B) are consistent with results from our recent modeling studies. Using network models of Hodgkin–Huxley neurons, we demonstrated that gamma and beta power increased in cortical circuits with low-dose propofol administration (38) and that as the dose was increased, gamma and beta activity coalesced into a coherent alpha oscillation through synchronization of thalamo-cortical interactions (39). This coalescence agrees with the traveling peak and the spatially coherent alpha activity we observed at LOC (Fig. 4D). Our model analysis suggests that this coalescence occurs as the cortex and thalamus mutually entrain through their reciprocal connections into tightly organized, spatially coherent oscillations in the alpha range (39).

Our current findings also suggest that propofol-induced gamma, beta, and coherent frontal alpha oscillations are likely not separate physiological phenomena but rather different dynamic regimes of thalamo-cortical networks whose activity tracks the level of arousal. Loss of gamma-band coherence has been reported to be associated with LOC (22, 40, 41). We observed changes in alpha-band power (Fig. 2) and coherence (Fig. 4) linked to LOC and ROC but did not see such effects in the gamma band.

The temporal coincidence between the changes in low-frequency (0.1–1 Hz) power and coherent alpha oscillations at LOC and ROC (Figs. 2 and 4) suggests that these phenomena may have a shared origin. There is a class of high-threshold thalamic

relay neurons that burst at alpha frequencies when depolarized but spike in a low-frequency burst pattern when hyperpolarized (42). Hyperpolarization of these neurons could explain the simultaneous changes in occipital alpha and low-frequency power at LOC and ROC. This hyperpolarization could occur via reduced excitatory input from cortex or brainstem, or from increased GABAergic inhibition from thalamic reticular nucleus.

The peak-max pattern (Fig. 5 and Fig. S3) resembles the slow oscillation which has been studied extensively in sleep (43), ketamine/xylazine anesthesia (44, 45), and, more recently, in studies of human single units during propofol-induced unconsciousness (46). In slow oscillations, surface-positive waves are associated with UP or ON states in which broad-band EEG, local field potential, and multiunit activity are all increased (44, 46–48). On the other hand, DOWN or OFF states are associated with periods of neuronal silence (44, 46–48). The slow oscillation is thought to reflect a state of reduced cortico-cortical functional connectivity (46, 49, 50). The spatial distribution and lack of spatial coherence we observed in the low-frequency oscillations are consistent with this idea (Fig. 4 and Fig. S2). The trough-max pattern could be an instantiation of the slow cortical potential, a category of low-frequency activity in which surface-negative deflections are associated with high-frequency activity (51). Anesthesia-induced phase–amplitude modulation has been studied previously (51–54). However, our results establish the existence of two distinct patterns of low-frequency phase modulation of the alpha/beta oscillation amplitudes and show that each pattern is linked to a different state of unconsciousness. The mechanism for the transition between the two patterns remains an open question.

Anteriorization, the frontal shift in EEG power in multiple bands, has also been associated with unconsciousness (20–24, 26, 52). We find that anteriorization begins before LOC and involves power increases in the alpha through gamma bands (traveling peak, Fig. 3) and increases in alpha band coherence at LOC (Fig. 4). During emergence, after ROC, anteriorization reverses, but frontal gamma power persists even after behavioral responses have returned (Fig. 3 and Fig. S2). These results suggest that

with a refractory period of several seconds (62), whereas propofol-induced alpha/beta oscillations appear more continuous in nature. This difference could reflect propofol's inhibitory effect on thalamic calcium-dependent hyperpolarization-activated currents (I_h) (63), which are thought to mediate the sleep spindle's transient shape and refractory period (64). Propofol-induced slow oscillations are associated with shorter periods of neuronal firing and longer periods of silence than sleep slow waves, suggesting a more profound degree of cortical impairment than seen with sleep (46). We speculate that, as a result, sleep slow waves might show less pronounced phase–amplitude modulation than the propofol-induced slow oscillation (peak-max).

EEG patterns similar to those described here during propofol-induced unconsciousness, including frontal alpha waves, low-frequency oscillations, and burst-suppression, can be observed in different coma states (1, 65). However, less is known about the spatiotemporal dynamics and mechanisms of these EEG patterns in coma, and further study will be required to make detailed comparisons with GA. More generally, systematic analyses comparing GA, sleep, coma, and other altered states of consciousness may yield important insights into the mechanisms underlying these phenomena.

Tracking Brain States of Patients Under GA. Anesthesiologists provide care to thousands of patients daily, but only about half use depth-of-anesthesia monitors (66). The EEG-derived indices reported by these monitors relate only indirectly to LOC, ROC, and unconsciousness. Hence, even when patients are monitored, their brain states are not known precisely (4). The standards for monitoring vital physiological variables in anesthesiology—heart rate, blood pressure, oxygen saturation, and temperature (67, 68)—have been critical for reducing morbidity, mortality, and malpractice premiums (69). Because there are no such standards for tracking brain states under GA (70), there is no principled way at present to prevent intraoperative awareness (4), postoperative delirium, or postoperative cognitive dysfunction.

The EEG signatures we have identified for propofol can be computed in real-time, are easy to recognize, and can be interpreted in a way that relates directly to the mechanisms through which this anesthetic is postulated to induce unconsciousness. The traveling peak and the trough-max pattern can be used to track transitions into and out of unconsciousness (Fig. 3*A* and *B*). Alpha coherence (Fig. 4) could be used as a marker of unconsciousness during surgeries such as carotid endarterectomies in patients that have a full EEG montage. The trough-max pattern offers a predictor of ROC (Fig. 5*A* and *B*), whereas the peak-max pattern (Fig. 5*A* and *B*) provides a signature of profound unconsciousness. When the peak-max pattern is present, our findings suggest that it is improbable that a patient will have awareness. Neither the trough-max nor the peak-max pattern can be detected by spectral or entropy-based analyses (3), because these quantities do not contain phase information. The bispectral statistic SyncFastSlow computed as part of the Bispectral Index (16) also is unable to detect these modulation patterns (36), most likely because the broad range of frequencies that are pooled together (0.5–47 Hz) effectively cancels out phase information (36, 71). However, because phase–amplitude modulation can be represented as a form of quadratic phase coupling (72), it could be estimated using properly structured bispectral techniques.

Studies of other anesthetics that combine experimental and modeling paradigms likewise could relate drug-specific EEG signatures to the mechanisms of drug action and the associated behavioral and brain states they produce. This deeper understanding of anesthetic neurophysiology will provide new insights into brain function and altered states of consciousness or arousal. It should also translate into more reliable approaches to monitoring the brain states of patients receiving GA and for tailoring drug dosing based on specific, real-time knowledge of these states. Such informed approaches are critical steps for establishing neurophysiologically based standards for brain-state monitoring during GA.

Materials and Methods

Subject Selection and Clinical Procedures. We studied 10 normal healthy volunteers, 18–36 y of age. These studies were approved by the Human Research Committee at the Massachusetts General Hospital. All subjects provided informed consent. All subjects were American Society of Anesthesiology Physical Status I with Mallampati Class I airway anatomy. In addition to standard preanesthesia assessments, we tested all subjects for normal hearing and performed a urine toxicology screen to ensure that subjects had not taken drugs that might interact adversely with propofol or confound the EEG or behavioral results. We administered a urine pregnancy test for each female subject to ensure that none was pregnant.

Before the start of the study, we required subjects to take nothing by mouth for at least 8 h. During the study, subjects breathed 30% oxygen by volume. We monitored each subject's heart rate with an electrocardiogram, oxygen saturation through pulse oximetry, respiration and expired carbon dioxide with capnography, and blood pressure through an arterial line. The arterial line also was used for blood sampling. To ensure subject safety, at least three anesthesiologists were present at each study: one was responsible solely for the medical management of the subject during the study, the second controlled the propofol administration, and the third performed blood sampling. When a subject became apneic, the first anesthesiologist assisted breathing with bag/mask ventilation. A phenylephrine infusion was used to maintain mean arterial pressure above a patient-specific level determined from the subject's baseline measurements.

Experimental Design and Procedures. For induction of unconsciousness, we used a computer-controlled infusion to achieve propofol target effect-site concentrations of 0, 1, 2, 3, 4, and 5 $\mu\text{g/mL}$ (Fig. 1*A*) (30, 73). We maintained each target effect-site concentration level for 14 min. We denoted the propofol concentration at which each subject stopped responding to button press as " C_{LOR} ." Emergence began at the end of the 5 $\mu\text{g/mL}$ level. To provide a gradual emergence, we reduced the propofol infusion rates in a stepwise fashion to achieve target effect-site concentrations of $C_{\text{LOR}} - 0.5 \mu\text{g/mL}$, $C_{\text{LOR}} - 1.0 \mu\text{g/mL}$, and $C_{\text{LOR}} - 1.5 \mu\text{g/mL}$, and 0 $\mu\text{g/mL}$, for 14 min each. We performed blood sampling for later propofol assays at the midpoint and end of each level.

Before each study, we acquired structural MRI for each subject (Siemens Trio 3 Tesla, T1-weighted magnetization-prepared rapid gradient echo, 1.3-mm slice thickness, $1.3 \times 1 \text{ mm}$ in-plane resolution, TR/TE = 2530/3.3 ms, 7° flip angle) and digitized scalp electrode positions (Polhemus FASTRACK 3D). During induction and emergence, we recorded EEGs using a 64-channel BrainVision MRI Plus system (Brain Products) with a sampling rate of 5,000 Hz, resolution 0.5 μV least significant bit (LSB), bandwidth 0.016–1000 Hz. We also recorded galvanic skin response, plethysmography (PowerLab; ADInstruments), and video (BrainVision Video Module; Brain Products).

Subjects were instructed to close their eyes throughout the study to avoid eye-blink artifacts in the EEG. Keeping the eyes closed also helped distinguish between normal awake, eyes-closed occipital alpha oscillations (34) and the frontal alpha oscillations associated with unconsciousness caused by propofol.

Subjects were presented a series of auditory stimuli during the study and asked to respond to these stimuli by button presses to assess level of conscious behavior. The stimuli, which consisted of either a verbal stimulus or an auditory click, were presented every 4 s in a repeating sequence of click-click-verbal-click-click, with a total of 210 stimuli per target effect-site concentration level. Verbal stimuli consisted either of the subject's name or a word (LIBRARY, CABINET, VEHICLE, TABLE, BUILDING, LADDER, PACKAGE), randomized with an equal number of name or word stimuli at each level. Words and names were recorded by a male native English speaker (P.L.P.). The click train was delivered binaurally, with 40-Hz clicks in the left ear and 84-Hz clicks in the right ear. Subjects were instructed to press one button if they heard their name and to press the other button if they heard any other stimulus. For click-train stimuli, subjects were instructed to wait until the end of the stimulus before responding so that auditory event-related potentials could be recorded without response artifacts. Analysis of these event-related potentials will be reported in a separate publication.

Click trains were constructed by modulating uniformly distributed white noise with a periodic ON/OFF trapezoid function (for 40-Hz clicks, 12.5-ms OFF period, 12.5-ms ON period, 2-ms rise time, 2-ms fall time; for 80 Hz clicks, 6-ms OFF period, 6-ms ON period, 1-ms rise time, 2-ms fall time). All stimuli were recorded at a sampling rate of 44.1 kHz. Stimuli were presented using Presentation software (Neurobehavioral Systems, Inc.) with ear-insert headphones (ER2; Etymotic Research) at ~ 81 decibels peak sound pressure level.

Button-press stimuli were recorded using a custom-built computer mouse with straps fitted to hold the first and second fingers in place over the mouse buttons throughout the study. The mouse also was lightly strapped to the

subject's hand using tape and an arterial line board to ensure that responses could be recorded accurately during emergence.

Behavioral Analysis. We estimated the probability of response to the click and verbal stimuli and the difference in probability of response by using Bayesian Monte Carlo methods to fit a state-space model to these data (31, 74). To perform group-level analyses, we aligned the behavioral data across subjects with respect to each subject's LOC time for induction and with respect to each subject's ROC time for emergence. We then pooled the responses within 20-s bins. The pooled data were used to estimate group-level probabilities of response using the state-space model.

EEG Preprocessing. We applied an anti-aliasing filter and down-sampled the EEG data to 500 or 250 Hz before analysis. An investigator experienced in reading EEGs (P.L.P.) visually inspected the data from each subject and excluded channels with noise or artifacts. We coregistered the electrode positions with MRI-based scalp-surface reconstructions obtained with Freesurfer (75) and remontaged EEG signals to a nearest-neighbor Laplacian reference, using distances along the scalp surface to weigh neighboring electrode contributions.

Spectral Analysis. We computed spectrograms using the multitaper method, with window lengths of $T = 2$ s with 1.9 s overlap, time-bandwidth product $TW = 2$, number of tapers $K = 3$, and spectral resolution of 2 Hz (32, 76). We computed group-level baseline-normalized spectrograms for induction and emergence by taking the median across subjects with the data aligned to the LOC and ROC time points, respectively. To determine if the group-level spectrogram was significantly greater than baseline, we performed a sign test at each time-frequency location, treating each subject as an independent sample.

To characterize the traveling peak, we first computed the group-level baseline- and total power-normalized spectra aligned at LOC (induction) and ROC (emergence) time points. We then computed the median, 25th, and 75th percentiles between 2 and 40 Hz at each time point and applied a random-walk fixed-interval smoother to each resulting time series (77). We estimated the state space observation variance by computing the sample variance of the first 10 s of each time series and estimated the random-walk state variance by taking the square of the end-to-end rate of change for each time series [i.e., $\sigma_{state}^2 = ((y_1 - y_N)/N)^2$, where N is the number of samples in the time series, and y_1 and y_N are the first and last samples in the time series, respectively]. We computed group-level scalp power distributions by taking the median across subjects. Scalp EEG plots were performed using the topoplots function in EEGLab (78).

Eigenvalue and Modal Projection Analyses. We performed an eigenvector decomposition analysis of the cross-spectral matrix to identify the principal modes of oscillation in the conscious and unconscious states and to analyze how activity within these principal modes changed through time. We estimated the cross-spectral matrices $P_{baseline}(f)$ and $P_{unconscious}(f)$ at each frequency f using the multitaper method (parameters as above) using data from the full baseline period, and segments of at least 5 min extending from LOC to ROC, respectively, for each subject. We divided each segment into nonoverlapping 2-s windows, and we computed the median over all windows of the real and imaginary parts of each entry in the cross-spectral

matrix (33). We performed an eigenvalue decomposition on this median cross-spectral matrix at each frequency. Each eigenvector describes a coherent spatial distribution or mode of oscillation, and the corresponding eigenvalue quantifies the power in this mode. We refer to the first eigenvector $u_1(f)$ at a given frequency f as the principal mode of oscillation for that frequency.

We used modal projection analysis to characterize how power within these principal modes changed as a function of time (33). For each Slepian-tapered, Fourier-transformed vector in each channel, $x(f, t)$, at frequency f and time window t (duration 20 s, nonoverlapping), we defined the modal projection as the power within the principal mode, normalized by total power:

$$MP(f, t) = \frac{|x^T(f, t)u_1(f)|^2}{|x(f, t)|^2}$$

We used a permutation-based procedure to assess statistical significance for the modal projection analysis. For each 20-s time window we applied a randomly selected circular time shift to the raw data from each channel. The shifted data then were subjected to the eigenvector and modal projection analysis described above. To generate a null distribution, we repeated this procedure 200 times with a new random time shift for each channel. To improve resolution we resampled the 200 permutation controls 500 times, with replacement. We used this null distribution to find the 95% confidence limit for significant modal projection for each subject at each time point and frequency. We averaged the 95% confidence limit across subjects and compared the average with the mean of the original global coherence. Time points and frequencies at which the mean modal projection was below the mean of the 95% confidence interval were determined to be nonsignificant (shown in gray in Fig. 4 B and D).

Phase-Amplitude Modulation Analysis. We analyzed the relationship between low-frequency phase (0.1–1 Hz) and alpha/beta (8–14 Hz) amplitude by calculating a phase-amplitude histogram, or “modulogram” (36). We down-sampled the EEG data to 250 Hz, then applied bandpass filters to construct narrow-band slow and alpha/beta signals (36). We then applied the Hilbert transform to each signal and computed the low-frequency oscillation phase $\Psi(t)$ and alpha oscillation amplitude $A(t)$. To construct the modulogram, we assigned each temporal sample to one of 18 equally spaced phase bins based on the value of $\Psi(t)$, averaging over 2-min epochs. The modulogram in each phase bin is the average of $A(t)$ for all samples within the bin, normalized by the average of $A(t)$ over the entire 2-min epoch. To assess statistical significance for the modulogram, we performed a permutation test, described in ref. 36.

ACKNOWLEDGMENTS. This work was supported by National Institutes of Health (NIH) Director's Pioneer Award DP1-OD003646 and NIH Grant R01-MH071847 (to E.N.B.), by NIH New Innovator Award DP2-OD006454 and K-Award K25-NS057580 (to P.L.P.), and by R01-EB006385 (to E.N.B., P.L.P., and K.F.K.W.) This work was also supported by the Massachusetts General Hospital Department of Anesthesia, Critical Care, and Pain Medicine, as well as the Harvard Catalyst and The Harvard Clinical and Translational Science Center (NIH Award UL1 RR 025758).

- Brown EN, Lydic R, Schiff ND (2010) General anesthesia, sleep, and coma. *N Engl J Med* 363(27):2638–2650.
- Brown EN, Purdon PL, Van Dort CJ (2011) General anesthesia and altered states of arousal: A systems neuroscience analysis. *Annu Rev Neurosci* 34:601–628.
- Palanca BJ, Mashour GA, Avidan MS (2009) Processed electroencephalogram in depth of anesthesia monitoring. *Curr Opin Anaesthesiol* 22(5):553–559.
- Avidan MS, et al.; BAG-RECALL Research Group (2011) Prevention of intraoperative awareness in a high-risk surgical population. *N Engl J Med* 365(7):591–600.
- Niedermeyer E, Lopes da Silva FH (2005) *Electroencephalography: Basic Principles, Clinical Applications, and Related Fields* (Lippincott Williams & Wilkins, Philadelphia), 5th Ed, pp xiii, 1309.
- Gibbs FA, Gibbs EL, Lennox WG (1937) Effect on the electroencephalogram of certain drugs which influence nervous activity. *Arch Intern Med* 60:154–169.
- Kiersey DK, Bickford RG, Faulconer A, Jr. (1951) Electro-encephalographic patterns produced by thiopental sodium during surgical operations; description and classification. *Br J Anaesth* 23(3):141–152.
- Faulconer A, Jr. (1952) Correlation of concentrations of ether in arterial blood with electroencephalographic patterns occurring during ether-oxygen and during nitrous oxide, oxygen and ether anesthesia of human surgical patients. *Anesthesiology* 13(4):361–369.
- Clark DL, Rosner BS (1973) Neurophysiologic effects of general anesthetics. I. The electroencephalogram and sensory evoked responses in man. *Anesthesiology* 38(6):564–582.
- Glass PS, et al. (1997) Bispectral analysis measures sedation and memory effects of propofol, midazolam, isoflurane, and alfentanil in healthy volunteers. *Anesthesiology* 86(4):836–847.
- Doi M, Gajraj RJ, Mantzaridis H, Kenny GN (1997) Relationship between calculated blood concentration of propofol and electrophysiological variables during emergence from anaesthesia: Comparison of bispectral index, spectral edge frequency, median frequency and auditory evoked potential index. *Br J Anaesth* 78(2):180–184.
- Schneider G, Gelb AW, Schmeller B, Tschakert R, Kochs E (2003) Detection of awareness in surgical patients with EEG-based indices—bispectral index and patient state index. *Br J Anaesth* 91(3):329–335.
- Li X, Cui S, Voss LJ (2008) Using permutation entropy to measure the electroencephalographic effects of sevoflurane. *Anesthesiology* 109(3):448–456.
- Schultz A, Siedenberg M, Grouven U, Kneif T, Schultz B (2008) Comparison of Narcotrend Index, Bispectral Index, spectral and entropy parameters during induction of propofol-remifentanyl anaesthesia. *J Clin Monit Comput* 22(2):103–111.
- Revueita M, et al. (2008) Validation of the index of consciousness during sevoflurane and remifentanyl anaesthesia: A comparison with the bispectral index and the cerebral state index. *Br J Anaesth* 101(5):653–658.
- Rampil IJ (1998) A primer for EEG signal processing in anesthesia. *Anesthesiology* 89(4):980–1002.
- Vlajkovic GP, Sindjelic RP (2007) Emergence delirium in children: Many questions, few answers. *Anesth Analg* 104(1):84–91.

18. Reddy SV (2012) Effect of general anesthetics on the developing brain. *J Anaesthesiol Clin Pharmacol* 28(1):6–10.
19. Krenk L, Rasmussen LS (2011) Postoperative delirium and postoperative cognitive dysfunction in the elderly - what are the differences? *Minerva Anesthesiol* 77(7):742–749.
20. Tinker JH, Sharbrough FW, Michenfelder JD (1977) Anterior shift of the dominant EEG rhythm during anesthesia in the Java monkey: Correlation with anesthetic potency. *Anesthesiology* 46(4):252–259.
21. Gugino LD, et al. (2001) Quantitative EEG changes associated with loss and return of consciousness in healthy adult volunteers anaesthetized with propofol or sevoflurane. *Br J Anaesth* 87(3):421–428.
22. John ER, et al. (2001) Invariant reversible QEEG effects of anesthetics. *Conscious Cogn* 10(2):165–183.
23. Feshchenko VA, Veselis RA, Reinsel RA (2004) Propofol-induced alpha rhythm. *Neuropsychobiology* 50(3):257–266.
24. Cimenser A, et al. (2011) Tracking brain states under general anesthesia by using global coherence analysis. *Proc Natl Acad Sci USA* 108(21):8832–8837.
25. Rampil IJ, Matteo RS (1987) Changes in EEG spectral edge frequency correlate with the hemodynamic response to laryngoscopy and intubation. *Anesthesiology* 67(1):139–142.
26. Supp GG, Siegel M, Hipp JF, Engel AK (2011) Cortical hypersynchrony predicts breakdown of sensory processing during loss of consciousness. *Curr Biol* 21(23):1988–1993.
27. Jääntti V, Yli-Hankala A, Baer GA, Porkkala T (1993) Slow potentials of EEG burst suppression pattern during anaesthesia. *Acta Anaesthesiol Scand* 37(1):121–123.
28. Chernik DA, et al. (1990) Validity and reliability of the Observer's Assessment of Alertness/Sedation Scale: Study with intravenous midazolam. *J Clin Psychopharmacol* 10(4):244–251.
29. Kearse LA, Jr., et al. (1998) Bispectral analysis of the electroencephalogram predicts conscious processing of information during propofol sedation and hypnosis. *Anesthesiology* 88(1):25–34.
30. Schnider TW, et al. (1999) The influence of age on propofol pharmacodynamics. *Anesthesiology* 90(6):1502–1516.
31. Smith AC, et al. (2004) Dynamic analysis of learning in behavioral experiments. *J Neurosci* 24(2):447–461.
32. Mitra P, Bokil H (2007) *Observed Brain Dynamics* (Oxford Univ Press, New York).
33. Wong KF, et al. (2011) Robust time-varying multivariate coherence estimation: Application to electroencephalogram recordings during general anesthesia. *Conf Proc IEEE Eng Med Biol Soc* 2011:4725–4728.
34. Redlich FC, Callahan A, Mendelson RH (1946) Electroencephalographic changes after eye opening and visual stimulation. *Yale J Biol Med* 18:367–376.
35. Tort AB, Komorowski R, Eichenbaum H, Kopell N (2010) Measuring phase-amplitude coupling between neuronal oscillations of different frequencies. *J Neurophysiol* 104(2):1195–1210.
36. Mukamel EA, Wong KF, Prerau MJ, Brown EN, Purdon PL (2011) Phase-based measures of cross-frequency coupling in brain electrical dynamics under general anesthesia. *Conf Proc IEEE Eng Med Biol Soc* 2011:1981–1984.
37. Kennedy D, Norman C (2005) What don't we know? *Science* 309(5731):75.
38. McCarthy MM, Brown EN, Kopell N (2008) Potential network mechanisms mediating electroencephalographic beta rhythm changes during propofol-induced paradoxical excitation. *J Neurosci* 28(50):13488–13504.
39. Ching S, Cimenser A, Purdon PL, Brown EN, Kopell NJ (2010) Thalamocortical model for a propofol-induced alpha-rhythm associated with loss of consciousness. *Proc Natl Acad Sci USA* 107(52):22665–22670.
40. Mashour GA (2004) Consciousness unbound: Toward a paradigm of general anesthesia. *Anesthesiology* 100(2):428–433.
41. Imas OA, Ropella KM, Ward BD, Wood JD, Hudetz AG (2005) Volatile anesthetics disrupt frontal-posterior recurrent information transfer at gamma frequencies in rat. *Neurosci Lett* 387(3):145–150.
42. Hughes SW, Crunelli V (2005) Thalamic mechanisms of EEG alpha rhythms and their pathological implications. *Neuroscientist* 11(4):357–372.
43. Crunelli V, Hughes SW (2010) The slow (<1 Hz) rhythm of non-REM sleep: A dialogue between three cardinal oscillators. *Nat Neurosci* 13(1):9–17.
44. Chauvette S, Crochet S, Volgushev M, Timofeev I (2011) Properties of slow oscillation during slow-wave sleep and anesthesia in cats. *J Neurosci* 31(42):14998–15008.
45. Steriade M, Nuñez A, Amzica F (1993) A novel slow (< 1 Hz) oscillation of neocortical neurons in vivo: Depolarizing and hyperpolarizing components. *J Neurosci* 13(8):3252–3265.
46. Lewis LD, et al. (2012) Rapid fragmentation of neuronal networks at the onset of propofol-induced unconsciousness. *Proc Natl Acad Sci USA* 109(49):E3377–E3386.
47. Csercsa R, et al. (2010) Laminar analysis of slow wave activity in humans. *Brain* 133(9):2814–2829.
48. Nir Y, et al. (2011) Regional slow waves and spindles in human sleep. *Neuron* 70(1):153–169.
49. Massimini M, et al. (2005) Breakdown of cortical effective connectivity during sleep. *Science* 309(5744):2228–2232.
50. Langheim FJ, Murphy M, Riedner BA, Tononi G (2011) Functional connectivity in slow-wave sleep: Identification of synchronous cortical activity during wakefulness and sleep using time series analysis of electroencephalographic data. *J Sleep Res* 20(4):496–505.
51. He BJ, Raichle ME (2009) The fMRI signal, slow cortical potential and consciousness. *Trends Cogn Sci* 13(7):302–309.
52. Murphy M, et al. (2011) Propofol anesthesia and sleep: A high-density EEG study. *Sleep* 34(3):283–91A.
53. Breshears JD, et al. (2010) Stable and dynamic cortical electrophysiology of induction and emergence with propofol anesthesia. *Proc Natl Acad Sci USA* 107(49):21170–21175.
54. Molae-Ardekani B, Senhadji L, Shamsollahi MB, Wodey E, Vosoughi-Vahdat B (2007) Delta waves differently modulate high frequency components of EEG oscillations in various unconsciousness levels. *Conf Proc IEEE Eng Med Biol Soc* 2007:1294–1297.
55. Blumenfeld H (2011) Epilepsy and the consciousness system: Transient vegetative state? *Neuro Clin* 29(4):801–823.
56. Alkire MT, Hudetz AG, Tononi G (2008) Consciousness and anesthesia. *Science* 322(5903):876–880.
57. Ku SW, Lee U, Noh GJ, Jun IG, Mashour GA (2011) Preferential inhibition of frontal-to-parietal feedback connectivity is a neurophysiologic correlate of general anesthesia in surgical patients. *PLoS ONE* 6(10):e25155.
58. Boly M, et al. (2012) Connectivity changes underlying spectral EEG changes during propofol-induced loss of consciousness. *J Neurosci* 32(20):7082–7090.
59. Dehaene S, Changeux JP (2011) Experimental and theoretical approaches to conscious processing. *Neuron* 70(2):200–227.
60. Franks NP, Zecharia AY (2011) Sleep and general anesthesia. *Can J Anaesth* 58(2):139–148.
61. Dehghani N, Cash SS, Halgren E (2011) Topographical frequency dynamics within EEG and MEG sleep spindles. *Clin Neurophysiol* 122(2):229–235.
62. Destexhe A, Contreras D, Steriade M (1998) Mechanisms underlying the synchronizing action of corticothalamic feedback through inhibition of thalamic relay cells. *J Neurophysiol* 79(2):999–1016.
63. Ying SW, Abbas SY, Harrison NL, Goldstein PA (2006) Propofol block of I(h) contributes to the suppression of neuronal excitability and rhythmic burst firing in thalamocortical neurons. *Eur J Neurosci* 23(2):465–480.
64. Destexhe A, Bal T, McCormick DA, Sejnowski TJ (1996) Ionic mechanisms underlying synchronized oscillations and propagating waves in a model of ferret thalamic slices. *J Neurophysiol* 76(3):2049–2070.
65. Brenner RP (2005) The interpretation of the EEG in stupor and coma. *Neurologist* 11(5):271–284.
66. Covidien (2011) BIS Education, Frequently Asked Questions: How often is BIS monitoring being used? Available at www.biseducation.com/faq1.aspx?mi=132.
67. Cooper JB, Newbower RS, Kitz RJ (1984) An analysis of major errors and equipment failures in anesthesia management: Considerations for prevention and detection. *Anesthesiology* 60(1):34–42.
68. Eichhorn JH, et al. (1986) Standards for patient monitoring during anesthesia at Harvard Medical School. *JAMA* 256(8):1017–1020.
69. Gaba DM (2000) Anaesthesiology as a model for patient safety in health care. *BMJ* 320(7237):785–788.
70. Anonymous; American Society of Anesthesiologists Task Force on Intraoperative Awareness (2006) Practice advisory for intraoperative awareness and brain function monitoring: A report by the american society of anesthesiologists task force on intraoperative awareness. *Anesthesiology* 104(4):847–864.
71. Miller A, Sleight JW, Barnard J, Steyn-Ross DA (2004) Does bispectral analysis of the electroencephalogram add anything but complexity? *Br J Anaesth* 92(1):8–13.
72. Nikias CL, Raghuveer MR (1987) Bispectrum estimation: A digital signal processing framework. *Proc IEEE* 75(7):869–891.
73. Shafer SL, Gregg KM (1992) Algorithms to rapidly achieve and maintain stable drug concentrations at the site of drug effect with a computer-controlled infusion pump. *J Pharmacokinetic Biopharm* 20(2):147–169.
74. Wong KF, et al. (2011) Bayesian analysis of trinomial data in behavioral experiments and its application to human studies of general anesthesia. *Conf Proc IEEE Eng Med Biol Soc* 2011:4705–4708.
75. Dale AM, Fischl B, Sereno MI (1999) Cortical surface-based analysis. I. Segmentation and surface reconstruction. *Neuroimage* 9(2):179–194.
76. Percival DB, Walden AT (1993) *Spectral Analysis for Physical Applications* (Cambridge Univ Press, New York).
77. Kitagawa G, Gersh W (1996) *Smoothness Priors Analysis of Time Series* (Springer, New York).
78. Delorme A, Makeig S (2004) EEGLAB: An open source toolbox for analysis of single-trial EEG dynamics including independent component analysis. *J Neurosci Methods* 134(1):9–21.